Systematic investigations into the role of ceramide subclass composition on lipid organization and skin barrier

Nadaban, A.

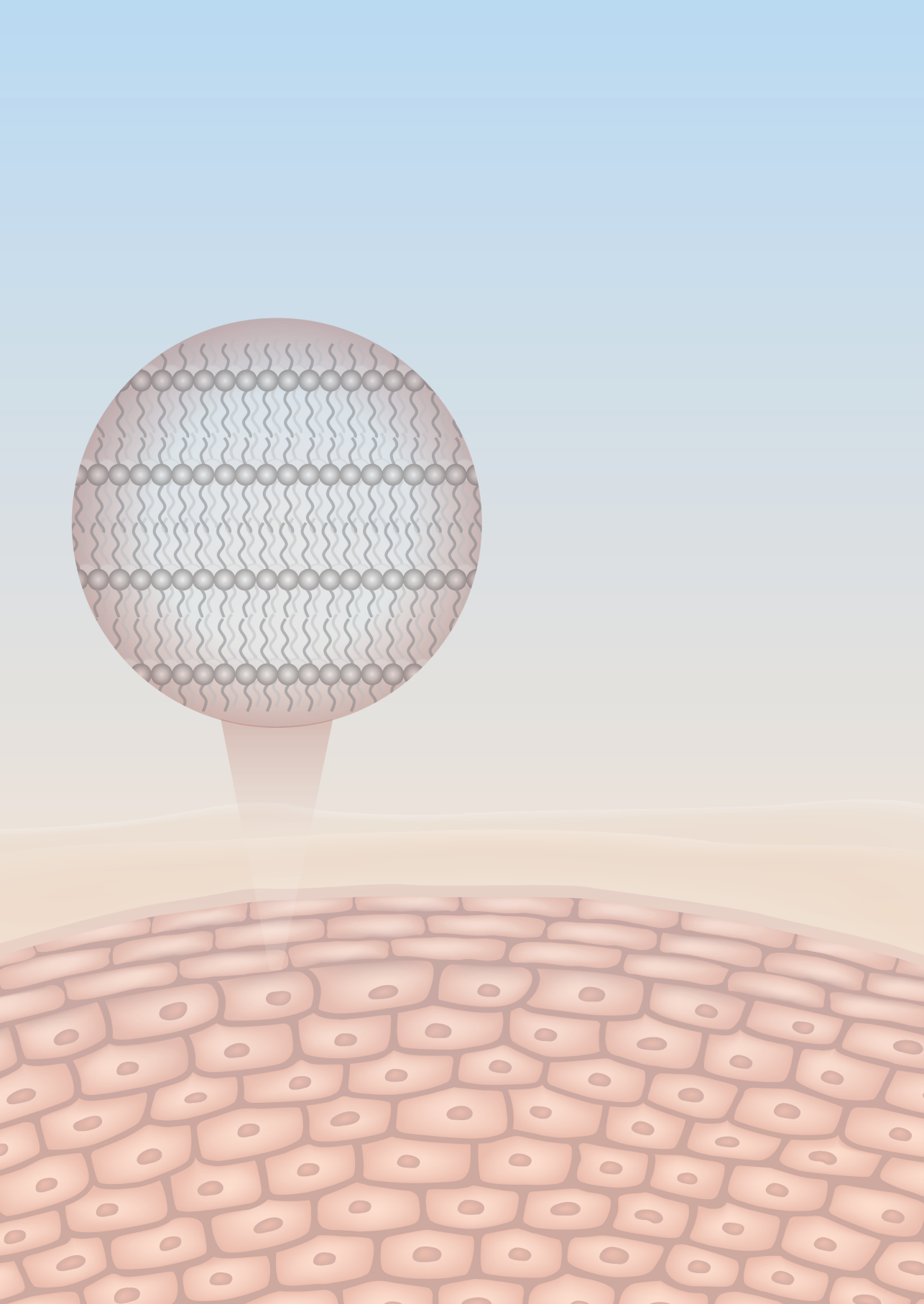

CHAPTER 2

Lesional skin of Seborrheic Dermatitis patients is characterized by skin barrier dysfunction and correlating alterations in the stratum corneum ceramide composition

Authors and affiliations:
Jannik Rousel[1,2], Andreea Nădăban[2], Mahdi Saghari[1,3], Lisa Pagan[1,3], Ahnjili Zhuparris[1,3,4], Bart Theelen[5], Tom Gambrah[1], Hein E.C. van der Wall[1], Rob J. Vreeken[6], Gary L. Feiss[7], Tessa Niemeyer-van der Kolk[1,3], Jacobus Burggraaf[1,2,3], Martijn B.A. van Doorn[1,8], Joke A. Bouwstra[2], Robert Rissmann[1,2,3]

[1]Centre for Human Drug Research, Leiden, The Netherlands
[2]Leiden Academic Centre for Drug Research, Leiden University, Leiden, The Netherlands
[3]Leiden University Medical Center, Leiden, The Netherlands
[4]Leiden Institute of Advanced Computer Science, Leiden University, Leiden, Netherlands
[5]Westerdijk Fungal Biodiversity Institute, Utrecht, The Netherlands
[6]Maastricht Multimodal Molecular Imaging Institute, Maastricht University, Maastricht, The Netherlands
[7]Cutanea Life Sciences, Wayne, Pennsylvania, USA
[8]Department of Dermatology, Erasmus Medical Centre, Rotterdam, The Netherlands

Adapted from: **Experimental Dermatology** (2024). 33(1): e14952

ABSTRACT

Background: Seborrheic dermatitis (SD) is a chronic inflammatory skin disease characterized by erythematous papulosquamous lesions in sebum rich areas such as the face and scalp. Its pathogenesis appears multifactorial with a disbalanced immune system, *Malassezia* driven microbial involvement and skin barrier perturbations. Microbial involvement has been well described in SD, but skin barrier involvement remains to be properly elucidated.

Objective: To establish whether barrier impairment is a critical factor of inflammation in SD alongside microbial dysbiosis.

Methods: A cross-sectional study was performed in 37 patients with mild-to-moderate facial SD. Their lesional and non-lesional skin was comprehensively and non-invasively assessed with standardized 2D-photography, optical coherence tomography (OCT), microbial profiling including *Malassezia* species identification, functional skin barrier assessments and ceramide profiling.

Results: Inflammation was established through significant increases in erythema, epidermal thickness, vascularization and superficial roughness in lesional skin compared to non-lesional skin. Lesional skin showed a perturbed skin barrier with an underlying skewed ceramide subclass composition, impaired chain elongation and increased chain unsaturation. Changes in ceramide composition correlated with barrier impairment indicating interdependency of the functional barrier and ceramide composition. Lesional skin showed significantly increased *Staphylococcus* and decreased *Cutibacterium* abundances but similar *Malassezia* abundances and mycobial composition compared to non-lesional skin. Principal component analysis highlighted barrier properties as main discriminating features.

Conclusions: SD is associated with skin barrier dysfunction and changes in the ceramide composition. No significant differences in the abundance of *Malassezia* were observed. Restoring the cutaneous barrier might be a valid therapeutic approach in the treatment of facial SD.

INTRODUCTION

Seborrheic dermatitis (SD) is an inflammatory, eczematous skin disease of the face and scalp with a multifactorial underlying pathophysiology. SD is characterized by the development of erythematous, scaly and itchy skin on seborrheic areas with high sebaceous gland activity such as the nasolabial folds, eyebrows and upper chest (supplemental Fig. S1) (1). The exact pathophysiology of SD remains unclear due to its multifactorial and complex aetiology. Three major interdependent driving factors of the aberrant immunological responses behind SD are I) individual susceptibility due to an imbalanced immune system leading to inflammation, II) cutaneous microbial dysbiosis with pronounced colonization by *Malassezia* species and III) a perturbed epidermal barrier(1,2).

While these three hallmarks all contribute towards the development of SD, much emphasis has been on the microbiome and especially the involvement of *Malassezia*. *Malassezia* is a commensal yeast which is regarded as a key pathogen due to its concurrence with lesional skin and the clinical response of SD to antifungals(3). It is hypothesized that the predilection of *Malassezia* for sebum-rich skin sites is due to its inability to perform *de novo* fatty acid synthesis, necessitating the processing of exogenous lipids which disturbs the epidermal barrier integrity and enables inflammation (4,5). While this provides rationale for why inflammation is limited to these areas, it has been shown that neither the amount of *Malassezia* (5,6) nor an increased level of sebum production (1,2,6) are strictly tied to the development of SD.

Due to the implication that external triggers such as *Malassezia* and its metabolites can penetrate the skin (7), the cutaneous barrier function itself has been proposed to be involved in SD pathogenesis (6). The epidermal barrier function is located in the stratum corneum which consists of layers of cornified cells embedded in a lipid matrix mainly composed of cholesterol, fatty acids and ceramides (8). Changes in the composition and consequently the lipid organization of this matrix directly impacts skin permeability (9,10). Barrier perturbations and simultaneous alterations of the lipid matrix composition, such as reduced chain length and changes in ceramide subclass composition, have been observed in other inflammatory skin diseases such as atopic dermatitis and psoriasis (11,12). This raised the question whether barrier repair can be exploited as a treatment option (13).

The apparent contribution of host immunity, the microbiome and cutaneous barrier to the development of SD warrants a multimodal assessment for phenotyping SD. In this study, we established cutaneous inflammation by clinical scoring complemented with imaging. We elucidated the bacterial and fungal composition as both are implicated in SD (14), with additional species-level profiling of *Malassezia*. Lastly, the cutaneous barrier function was characterized in-depth by trans-epidermal water loss (TEWL) measurements complemented with ceramide profiling using lipidomic analysis. This might yield new insights into how these modalities are implicated in disease.

METHODS

An extended version of the methods can be found in the supporting information.

Study design and population

The study was conducted at the Centre for Human Drug Research (Leiden, the Netherlands) from November 2018 to January 2020 following the Declaration of Helsinki principles after approval by the medical ethics committee Stichting Beoordeling Ethiek Biomedisch Onderzoek (Assen, the Netherlands). Patients gave written informed consent prior to participation in the study. The use of SD medication was prohibited prior to enrolment for a period of two weeks for topical treatments, including dandruff shampoos, three weeks for phototherapy and four weeks for systemic treatments. In total, 37 patient exhibiting mild-to-moderate SD defined by an Investigator's Global Assessment (IGA) score of 2 to 3 after verification by a dermatologist were included and assessments performed during a single visit. Due to the heterogeneous presentation of SD and the invasiveness of assessments, assessments are performed on different sites of the face as listed in supplemental table S1-3. See Supplementary Material for further details.

Clinical characteristics

Disease severity was scored using the Seborrheic Dermatitis and Severity Index (SDASI) adapted from Baysal, *et al.* (2004) (15), 5-point IGA and percentage affected body surface area (%BSA). Patient reported outcomes included the 0 – 100 Numeric Rating Scale (NRS) itch, 5-Domain Itch Questionnaire(16) and Dermatology Life Quality Index (DLQI) (17,18). See Supplementary Material for further details.

Standardized photography

Standardized two dimensional cross-polarized images of the face were taken using a VISIA-CR (Canfield Scientific, New Jersey, United States). Erythema Index calculations were performed based on a method by Yamamoto, *et al.* (2008) (19). See Supplementary Material for further details.

Optical Coherence Tomography

Lesional and non-lesional skin was imaged by Vivosight Dx optical coherence tomography (OCT) (Michelson Diagnostics, Kent, United Kingdom) and epidermal thickness, superficial roughness and average epidermal vascularization were determined. See Supplementary Material for further details.

Microbiome composition

Skin swabs were collected by rubbing the skin for 10 seconds. Swabs were extracted and 16s rRNA and internal transcribed spacer (ITS) sequencing was performed to determine the bacterial and fungal composition, respectively. After genus level classification,

microbes contributing <1% of the total were excluded and relative abundances determined. See Supplementary Material for further details.

Malassezia culturing

Agar plates with modified Dixon medium were pressed against the skin for 20 seconds and cultured for *Malassezia*. *Malassezia* species determination by matrix-assisted laser desorption ionization-time of flight mass spectrometry (MALDI-TOF MS) was performed on mycological isolates as described by Kolecka *et al.* (2014) (20). See Supplementary Material for further details.

Skin barrier integrity by trans-epidermal water loss

Subjects were allowed to acclimatize to controlled environmental conditions (humidity <60%, temperature 22±2 °C) in rested state for at least 15 minutes prior to measurements. TEWL was measured using an AquaFlux AF200 (Biox Systems Ltd., London, United Kingdom). See Supplementary Material for further details.

Skin barrier lipidomics

Stratum corneum was harvested with 4 polyphenylene sulfide tape (Nichiban, Tokyo, Japan) after applying pressure using a D500 D-squame Pressure Instrument (CuDerm Corporation, Dallas, TX, United States). Tapes were extracted and the ceramide fraction analyzed through a validated Liquid Chromatography-Mass Spectrometry (LC-MS) setup as described by Boiten *et al.* (2016) (21). Supplemental figure S2 lists the 12 most prevalent ceramide classes included in the analysis using the nomenclature by Motta *et al.* (1993) (22). Sebum levels were determined using a Sebumeter SM815 (Courage+Khazaka, Köln, Germany). See Supplementary Material for further details.

Statistical analysis

Data visualization and statistical testing was performed using Prism 9 (Graphpad Software, San Diego, California, United States). 2-way ANOVA, or a mixed effects model in the case of missing data points, was performed using Bonferroni's multiple comparison test in the case of multiple variables and paired t-test in the case of two variables. P-values are denoted as ns: $P>0.05$, *: $P\leq0.05$, **: $P\leq0.01$, ***: $P\leq0.001$. Integrative data graphing by principal component analysis (PCA) and min-max radar plotting has been performed through Python version 3.8.0 (Python Software Foundation, Wilmington, Delaware, United States). See Supplementary Material for further details.

RESULTS

In total, 37 patients were enrolled into the study. The patient population exhibited mild-to-moderate SD as shown by a SDASI score of 7.0 ± 4.3 and IGA score of ≤ 3 for 97% of all patients (Table 1). Patient reported disease burden was rated mild-to-moderate as evident from the DLQI (7.2±5.5/30; "moderate effect on patient's life"), average itch rating scale (23.6± 22.5/100) and 5-Domain itch scale rating (11.6± 3.2/25).

Table 1. Baseline demographics including clinical scoring and patient reported outcomes from the study population. The minimal and maximal values are indicated among their respective scores. BMI; Body Mass Index, SD; standard deviation.

Subjects (n)		37
Age (years)		37.8 ± 15.6
BMI (kg/m^2)		25.4 ± 3.4
Sex	Female	5 (13.5%)
	Male	32 (86.5%)
Race	Asian	1 (2.7%)
	Mixed (White, African)	1 (2.7%)
	Latino	1 (2.7%)
	White	34 (91.9%)
Fitzpatrick skin type	1	4 (10.8%)
	2	19 (51.4%)
	3	13 (35.1%)
	4	1 (2.7%)
	5	0 (0.0%)
	6	0 (0.0%)
Seborrheic Dermatitis Area and Severity index (0 – 45) (Mean ±SD)		7.0 ± 4.3
Investigator's Global Assessment	1 (almost clear)	4 (10.8%)
	2 (mild)	19 (51.4%)
	3 (moderate)	13 (35.1%)
	4 (severe)	1 (2.7%)
Affected body surface area (%) (Mean ±SD)		1.3 ± 0.7
Dermatology Life Quality Index (0 – 30) (Mean ±SD)		7.2 ± 5.5
Average Itch Numeric Rating scale (0 - 100) (Mean ±SD)		23.6 ± 22.5
5-Domain Itch Scale (5 - 25) (Mean ±SD)		11.6 ± 3.2

Inflammation

Apart from clinical scoring, hallmarks of inflammation were assessed using standardized 2D-photography and OCT. Lesional skin had a significantly higher erythema index compared to non-lesional skin (67.62 AU vs. 49.19 AU, P≤0.001, Fig. 1A). Despite high epidermal disorganization hampering the localization of the dermal-epidermal junction in multiple measurements, the epidermis of lesional skin was significantly thicker compared to non-lesional skin (0.15 mm vs. 0.10 mm, P≤0.001, Fig. 1B). Superficial roughness of the skin was significantly increased in lesional skin (0.013 AU vs 0.009 AU, P≤0.001, Fig. 1C). Higher superficial vascularization was observed in lesional skin compared to non-lesional skin at a shallow skin depth of 0.1 to 0.25 mm (P≤0.05-0.001, Fig. 1D) with no significant differences at greater depths. This culminates to an increased average vascularization between 0.1 to 0.25 mm of 0.079 in lesional skin compared to 0.058 in non-lesional skin (P≤0.001, supplemental Fig. S3).

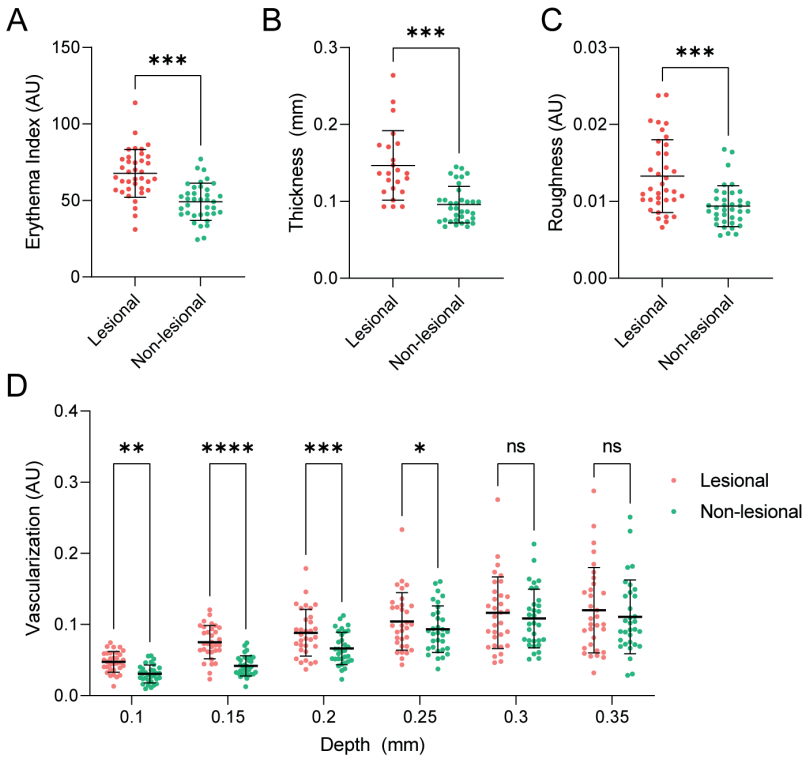

Figure 1. Erythema index as determined by standardized photography (A) and the epidermal thickness (B), superficial roughness (C) and the degree of vascularization at different depths in the epidermis (D) as determined by optical coherence tomography of lesional and non-lesional skin. Epidermal thickness could only be determined in 23 of 37 lesional and 34 of 37 non-lesional measurements. AU; Arbitrary Units, NS; not significant.

Microbiome

After establishing the presence of inflammation, the facial microbial composition was investigated using 16s rRNA and ITS sequencing for the bacterial and fungal microbiome, respectively.

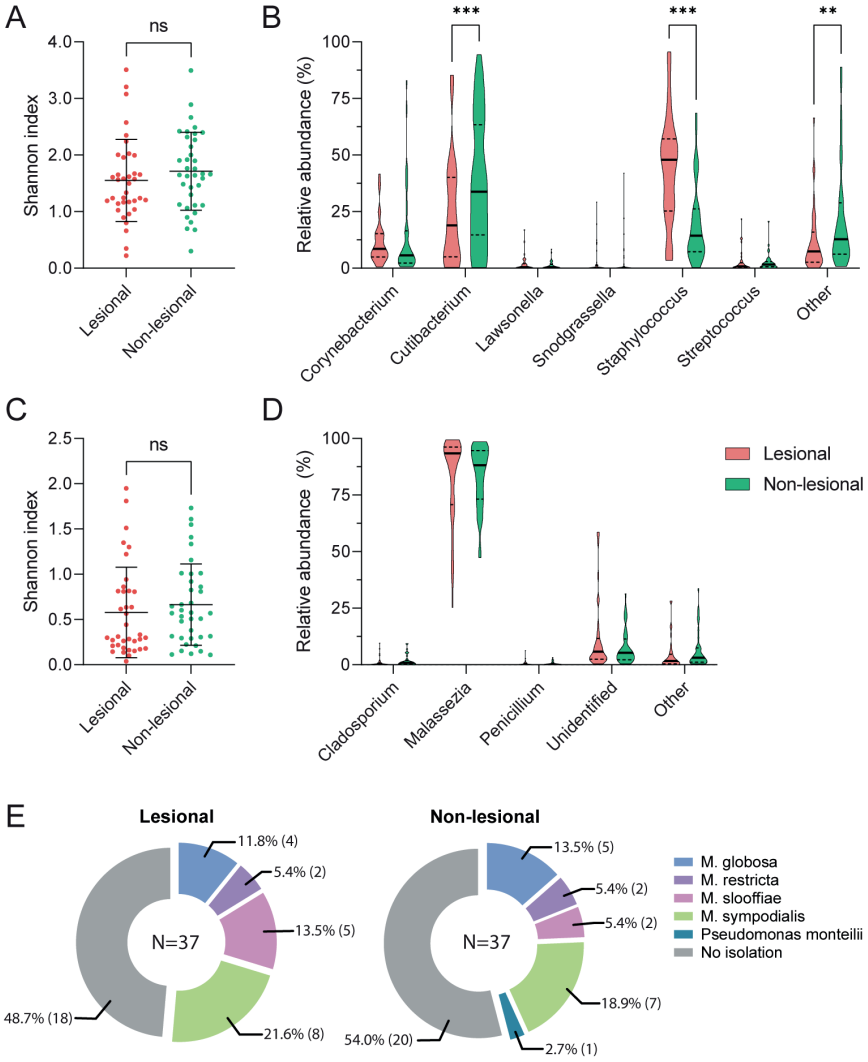

Figure 2. Bacterial Shannon diversity index (A) and composition of the bacterial microbiome (B) by 16s rRNA sequencing along with the fungal Shannon diversity index (C) and composition of the fungal microbiome (D) by ITS sequencing. The presented genera are filtered for minimal prevalence of 1% over all samples and presented relative to the total amount of microbes detected per analysis. Presence of different *Malassezia* species per site after isolation with contact plates and subsequent MALDI-TOF analysis (E). None of the samples yielded two or more different isolates.

Neither Shannon indexes showed a significant difference between lesional and non-lesional skin sites (1.55 vs 1.71, P>0.24 and 0.58 vs 0.66, P>0.23, for bacteria and fungi respectively, Fig. 2A, 2C), indicating biodiversity on average did not differ between skin sites. However, *Staphylococcus* was significantly overrepresented and *Cutibacterium* significantly underrepresented in lesional skin compared to non-lesional skin (44.05% vs 19.50% and 23.04% vs 38.20%, respectively, P≤0.001, Fig. 2B). The mycobiome proved small with only 3 genera present over the detection thresholds used (Fig. 2D), of which over 80% comprised of *Malassezia* hits in both lesional and non-lesional skin without any significant differences (82.20% vs. 83,52%, P>0.05). Due to the limitations associated with reliable identification of *Malassezia* at the species-level using ITS-sequencing, axenic culture plates were taken and subsequent MALDI-TOF MS was performed as a more specific qualitative alternative. Using *Malassezia* specific protocols successful isolation and identification of 16 from 37 lesional and 18 from 37 non-lesional samples was possible. No clear differences were observed between skin sites with *M. sympodialis* being the most prevalent at both sites (21.6% and 18.9% on lesional and non-lesional skin, respectively), followed by *M. slooffiae* (13.5%) on lesional and *M. globosa* (13.5%) on non-lesional skin (Fig. 2E).

Skin barrier

Finally, the skin barrier was studied as it represents the interface between external pathogens and the established epidermal inflammation. TEWL was used as an endpoint for skin barrier integrity and was significantly higher in lesional skin compared to non-lesional skin indicating an impaired barrier function (35.89 g/m^2/hr vs 21.27 g/m^2/hr, p>0.001, Fig. 3A). Sebum levels were not significantly different between lesional and non-lesional skin (90.70±54.93 vs 82.78±53.29, p=0.521, supplemental Fig. S4). The relative abundance was determined of all twelve major ceramide classes. The lesional ceramide profile showed a significant increase in Cer[NS] and Cer[AS] (17.25% vs 11.86% and 16.99% vs 10.61%, respectively, P≤0.001) and significantly decreased abundance of Cer[NdS], Cer[EOS] (7.15% vs 8.06% and 2.52% vs 3.51%, respectively, P≤0.01) and Cer[NP], Cer[NH], Cer[AP] (10.58% vs 14.29%, 10.87% vs 12.23%, 13.22% vs 16.03%, respectively, P≤0.001, Fig. 3B) compared to non-lesional skin. The abundance of other classes was not significantly different.

The skewing of ceramide subclass synthesis can be easily interpreted by comparing the abundance of Cer[NS] and Cer[NP]. Indeed, alterations in lipid processing were evident from a significant increase of the Cer[NS]:Cer[NP] ratio in lesional compared to non-lesional skin (1.68 vs 0.87, P≤0.001, Fig. 3C). Additionally, the presence of Cer[NSc34], a Cer[NS] species with a total chain length of 34 carbons, was significantly elevated in lesional compared to non-lesional skin (8.19% vs 5.10%, P≤0.001, Fig. 3D). Using the monounsaturation in Cer[NS] as an indicator for the overall monounsaturation, ceramides at lesional skin sites were further impacted by a higher degree of unsaturation compared

to non-lesional skin (7.32% vs 3.71%, P≤0.001, Fig. 3E). Lastly, lipid elongation was impaired in lesional skin as evident from a decreased average total carbon chain length of the ceramides compared to non-lesional skin (42.64 carbons vs 43.85 carbons, P≤0.001, Fig. 3F).

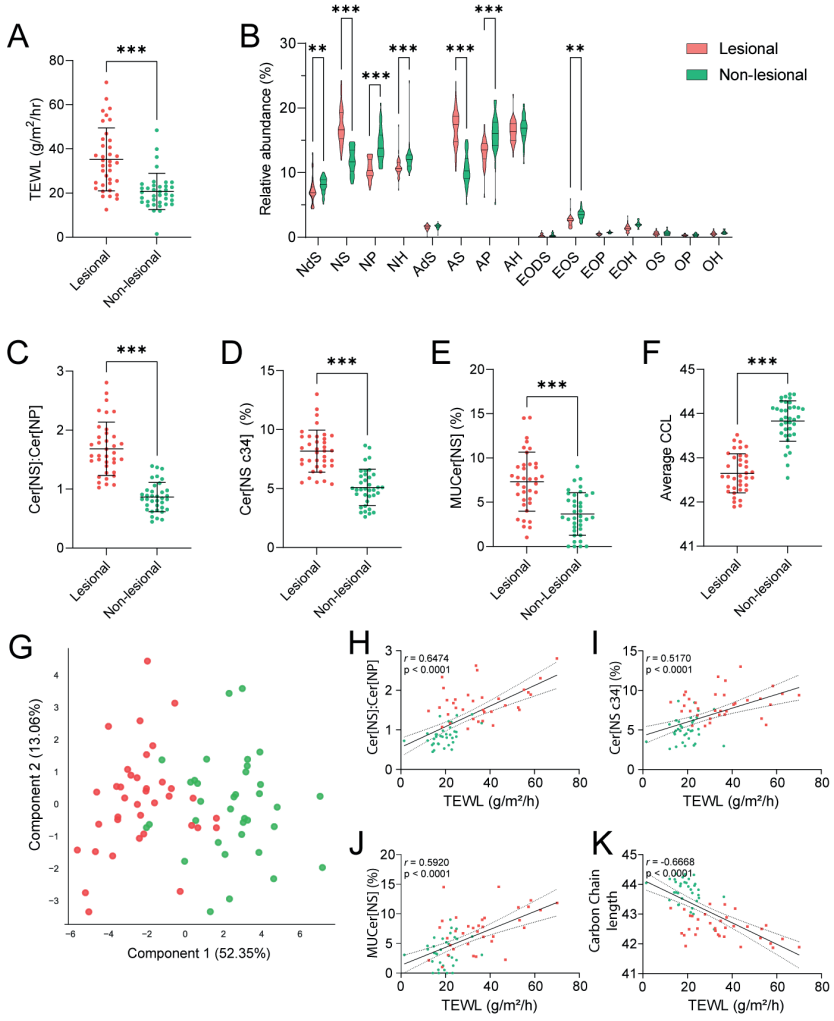

Figure 3. Barrier parameters of lesional compared to non-lesional skin demonstrate impaired barrier function in lesional skin. Functional barrier integrity is measured by trans-epidermal water loss (A). The ceramide profile is depicted after grouping individual ceramides per subclass (B), with the ratio between the abundance of Cer[NS] and Cer[NP] highlighted (C). The abundance of short ceramide species Cer[NSc34] (D) and degree of unsaturation (E) within Cer[NS] is shown. The average carbon chain length (CCL) of the combined sphingosine base and fatty acid tail within the non-Cer[EO] moiety is depicted (F). PCA analysis using all individual detected saturated ceramides yields two distinct population (G). Axes list the percentage of variance explained by the first two principal

components, with the proximity of datapoints indicating similarity between samples. Correlations between TEWL and Cer[NS]:Cer[NP] (H), percentage Cer[NSc34] (I), percentage of unsaturation (J) and CCL (K) are shown with a line representing the optimal fit from linear regression analysis and 95% confident interval and Pearson's correlation coefficient. TEWL; Trans-Epidermal Water Loss, MUCer; monounsaturated ceramide, CCL; carbon chain length, hr: hour.

Visualization of the roughly 300 individual ceramide responses using dimension reduction analysis by PCA showed two distinguishable populations when stratifying for skin site (Fig. 3G). This indicates the ceramide profile of lesional skin is alike between subjects, but differs from non-lesional skin. Plotting the TEWL values against ceramide parameters revealed a positive correlation for ceramide Cer[NS]:Cer[NP] ratio (*r*=0.6474), amount of Cer[NSc34] (*r*=0.5170) and degree of unsaturation (*r*=0.5920) and a negative correlation against the ceramide chain length (*r*=-0.6668) (Fig. 3H-K).

Integration of results

Integration of quantitative clinical characteristics (Fig. 1A, C, D), microbial properties (Fig. 2A-D) and barrier parameters (Fig. 3A-F) was performed using the entire dataset. The resulting PCA shows two distinguishable sets of data points with minimal overlap when stratifying for site (Fig. 4A). The abundance of Cer[NS], the carbon chain length and the Cer[NS]:Cer[NP] ratio contribute most to the overall differential analysis (supplemental table S4). Min-max normalized visualisation of the most significant findings in a radar chart underline that the biggest differences are observed in the barrier compartment followed by inflammation (Fig. 4B). Small differences between lesional and non-lesional skin were observed in the microbial parameters, with only the abundance of *Staphylococcus* being markedly different.

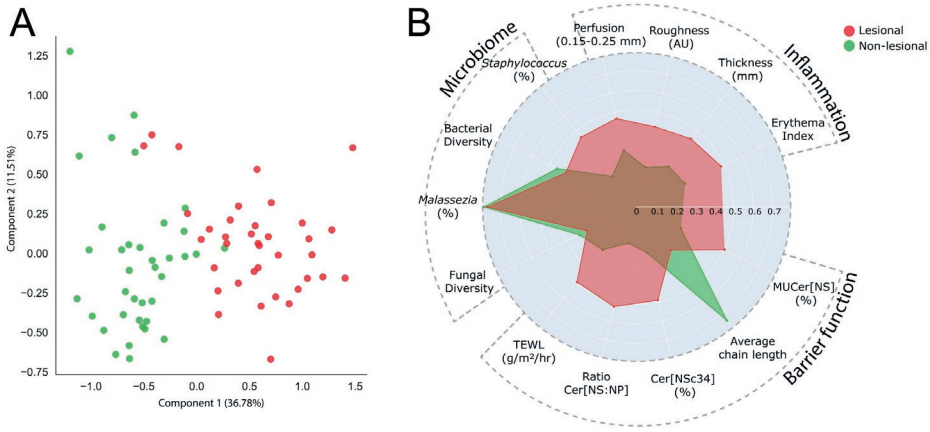

Figure 4. Principal component analysis (PCA) of lesional and non-lesional skin using all individual datapoints (A). Axes list the percentage of variance explained by the first two principal components. Integrative visualization of major contributors within the three different axes by radar chart (B). The

distance of a datapoint from the center represent the average value per parameter per site compared to the average value per parameter of both sites. AU; arbitrary units, TEWL; Trans-Epidermal Water Loss, MUCer; monounsaturated ceramide, CCL; carbon chain length, hr: hour

DISCUSSION

SD is a multifactorial disease in which the interplay between the cutaneous microbiome, especially the presence of *Malassezia*, impaired skin barrier function and abnormal immunological responses seem integral to its pathogenesis (1). In this study we comprehensively and non-invasively characterized the clinical representation of mild-to-moderate SD. We demonstrated a profound involvement of cutaneous barrier dysfunction with only small alterations in the microbiome, including the abundance of *Malassezia*, based on differences between lesional and non-lesional skin. This trial was performed in a sizeable number of 37 patients with similar disease burden after appropriate wash-outs and screening.

Inflammation objectively quantified by OCT and standardized imaging

Visual assessment of SD, which includes the evaluation of erythema, is frequently used in daily clinical practice for disease monitoring. However, visual examination of the skin can be hampered by limited sensitivity, observer bias and overall intra- and inter-rater variability (23,24). Therefore, we selected an objective approach to quantify cutaneous inflammation. Digitalized erythema assessments have been reported but not applied to SD (25–28). Here, standardized cross-polarized light photography is used to capture consistent images and enhanced erythema (29), resulting in a clear differentiation between lesional and non-lesional skin. Optical biopsies by OCT enabled the determination of additional (sub)cutaneous parameters. Inflammatory characteristics such as increased perfusion (30) and epidermal thickness, corresponding to acanthosis(31,32), were observed in lesional skin. Furthermore, a rougher lesional skin surface corresponds to the scaly phenotype of the disease (1). Increased blood flow and epidermal thickness have been observed by OCT in the involved skin of psoriasis and atopic dermatitis patients compared to uninvolved skin and healthy controls (33,34). Stand-alone, but also combined, standardized photography and OCT qualify as valuable non-invasive tools which enable sensitive and selective endpoints for disease monitoring and detection of treatment responses in clinical trials (35).

Malassezia and Staphylococcus dominate the lesional microbiome

Bacterial analysis of the skin surface showed an increased abundance of *Staphylococcus* and decreased abundance of *Cutibacterium* on lesional skin which concurs with previous SD profiling studies (14,36). *Staphylococcus*, and especially *S. aureus*, is considered to be a

pro-inflammatory mediator in atopic dermatitis(37). While limited phylogenetic resolution prevents the identification of *S. aureus* in this study, the observed increase of *Staphylococcus* combined with reports that *S. aureus* is more abundant in SD patients compared to healthy controls might indicate bacterial involvement in SD pathogenesis (38). Despite reports of bacterial involvement in SD, microbial involvement remains primarily focused on *Malassezia* as a key pathogen. However, no differences were observed between the abundance of *Malassezia* on lesional and non-lesional skin. This is in accordance with findings showing the presence of *Malassezia* is neither limited to lesional skin nor SD patients (3,6,14). Additionally, facial skin of healthy volunteers also showed a seemingly small and *Malassezia* dominated mycobiome (39,40). Although it is hypothesized that specific *Malassezia* species might be responsible for instigating inflammation as virulence factors differ between *Malassezia* species (41–43), no significant differences on species level were observed in this study. Culturing led to successful isolation of *Malassezia* species in approximately half of the subjects, illustrating the known challenges of isolating *Malassezia* from clinical samples (44). Except for *M. slooffiae*, all species are relatively frequently isolated from healthy and SD skin (45). Remarkably, *M. slooffiae* has been reported to have little virulence when directly compared to *M. globosa* and *M. sympodialis* (42). However, intra-species variation in virulence has been reported indicating that microbial activity rather than abundance is an important factor for the association of specific species to lesional skin (46,47). Based on these results, it seems too straightforward to attribute SD pathogenesis to the presence of *Malassezia* alone.

Substantial functional and compositional barrier alterations

Until now, the limited studies that have demonstrated functional barrier impairment in SD have neglected the lipid compartment as barrier component (48,49). In this study, we show a substantially impacted barrier in lesional skin on functional grounds by TEWL and demonstrate concomitant changes in the ceramide profile. These compositional changes correlated with the degree of barrier impairment as judged by TEWL. In line with our study in SD, changes in the Cer[NS]:Cer[NP] ratio(50), degree of unsaturation (51), ceramide chain length (12,52) and presence of extremely short chain Cer[NSc34] (12,51,53,54) in lesional skin have been observed in atopic dermatitis where barrier involvement is firmly established. These changes to the lipid profile appear to be induced by inflammation as lipid alterations can be evoked by atopic dermatitis and psoriasis associated pro-inflammatory cytokines *in vitro* (55–57) and normalize in response to anti-inflammatory treatment in atopic dermatitis patients (58). Whether these alterations are therefore primarily linked to inflammation and only coincide with barrier dysfunction has been investigated in mechanistic studies using lipid model systems. Lacking an inflammatory component, these models have shown that increased Cer[NS] (59,60), increased

unsaturation (61) and decreased lipid chain length (62) directly increase permeability. Additionally, studies in healthy volunteers have shown Cer[NS]:Cer[NP] ratios in the face comparable to non-lesional skin without a location-dependent effect on Cer[NSc34] abundances (63,64). It is of note that total ceramide levels can change with age and seasons as demonstrated in healthy skin and acne, but without much effect on the relative ceramide subclass composition as reported on in the current study (63,65,66). Additionally, the impact of these factors might be limited as patients serve as their own control. The predilection of SD lesions with areas known for increased water loss such as the mouth, eyelids and nasolabial folds might be confounding for the increased TEWL (49,67). Indeed, healthy volunteers have shown TEWL values at the nasolabial fold that approach the lesional values observed in this study with comparable TEWL values at the cheek or forehead, sites where non-lesional measurements were often conducted(68,69). Therefore, increased TEWL values in lesional skin may not reflect barrier impairment but rather indicate differences in normal physiological functioning between skin sites. However, the concurrent correlations between the TEWL values and ceramide composition reaffirm the interdependence of SD functional barrier impairment and ceramide-compositional alterations.

Integrative data analysis emphasizes importance of barrier dysfunction

An integrative approach was taken to visualize the data after investigating the three hallmarks of SD separately. Using PCA, we elucidated which parameters of our dataset predominantly contribute to the SD phenotype. The abundance of Cer[NS] and ceramide chain length showed to be the most important discriminating features. Indeed, the radar plot directs emphasis towards barrier function with little differences in the micro- and mycobiome. While the contribution of *Malassezia* seems to be negligible when only considering relative abundances, it should be re-emphasized that SD appears to be neither caused solely by barrier dysfunction nor microbial involvement but rather by the interplay between factors. This finding correlates with the shifting belief in literature that *Malassezia* might not be solely responsible for causing SD (5,6). This highlights the added value of a multimodal and integrative approach to disease profiling which enables in-depth characterization with the possibility to unravel part of pathogenesis (35).

CONCLUSION

In conclusion, this study demonstrates the importance of the barrier-inflammation axis in mild-to-moderate SD which seems to be more prominently involved compared to the microbiome. While not incorporating an internal healthy control group, our results are compared thoroughly with prior research in healthy volunteers through literature. Moreover, the results agree with and support existing literature regarding inflammation and microbial involvement in SD while complementing the current understanding of

barrier dysfunction in SD. Barrier impairment parallels that of atopic dermatitis where emollients are used effectively(70). Treating SD by improving the skin barrier function has been proposed as a potential adjuvant therapy(71), but the management of SD remains focused on anti-inflammatory and anti-fungal treatments(72). Taken together, the incorporation of emollients, humectants or other barrier repair agents should not be neglected in the management of SD and might support current treatment modalities.

REFERENCES

1. Borda, L.J., Wikramanayake, T.C. (2015). Seborrheic Dermatitis and Dandruff: A Comprehensive Review. *J Clin Investig Dermatol*. 3(2).
2. Goldenberg, G. (2013). Optimizing Treatment Approaches in Seborrheic Dermatitis. *J Clin Aesthet Dermatol*. 6(2):44.
3. del Rosso, J.Q., Kim, G.K. (2009). Seborrheic Dermatitis and Malassezia species: How Are They Related? *J Clin Aesthet Dermatol*. 2(11):14.
4. Juntachai, W., Oura, T., Murayama, S.Y., Kajiwara, S. (2009). The lipolytic enzymes activities of Malassezia species. *Med Mycol*. 47(5):477–84.
5. Adalsteinsson, J.A., Kaushik, S., Muzumdar, S., Guttman, E., Ungar, J. (2020). An update on the microbiology, immunology and genetics of seborrheic dermatitis. *Exp Dermatol*. 29(5):481–9.
6. Wikramanayake, T.C., Borda, L.J., Miteva, M., Paus, R. (2019). Seborrheic dermatitis—Looking beyond Malassezia. *Exp Dermatol*. 28(9):991–1001.
7. Goh, J.P.Z., Ruchti, F., Poh, S.E., Koh, W.L.C., Tan, K.Y., Lim, Y.T., et al. (2022). The human pathobiont Malassezia furfur secreted protease Mfsap1 regulates cell dispersal and exacerbates skin inflammation. *Proc. Natl. Acad. Sci.* 119(49):e2212533119.
8. Proksch, E., Brandner, J.M., Jensen, J.M. (2008). The skin: an indispensable barrier. *Exp Dermatol*. 17(12):1063–72.
9. Uche, L.E., Gooris, G.S., Bouwstra, J.A., Beddoes, C.M. (2021). High concentration of the ester-linked ω-hydroxy ceramide increases the permeability in skin lipid model membranes. *Biochimica et Biophysica Acta (BBA) – Biomembranes*. 1863(1):183487.
10. Beddoes, C.M., Gooris, G.S., Barlow, D.J., Lawrence, M.J., Dalgliesh, R.M., Malfois, M., et al. (2022). The importance of ceramide headgroup for lipid localisation in skin lipid models. *Biochimica et Biophysica Acta (BBA) - Biomembranes*. 1864(6):183886.
11. Ishikawa, J., Narita, H., Kondo, N., Hotta, M., Takagi, Y., Masukawa, Y., et al. (2010). Changes in the Ceramide Profile of Atopic Dermatitis Patients. *J. Invest. Dermatol*. 130(10):2511–4.
12. Janssens, M., van Smeden, J., Gooris, G.S., Bras, W., Portale, G., Caspers, P.J., et al. (2012). Increase in short-chain ceramides correlates with an altered lipid organization and decreased barrier function in atopic eczema patients. *J Lipid Res*. 53(12):2755–66.
13. Elias, P.M. (2022). Optimizing emollient therapy for skin barrier repair in atopic dermatitis.*Annals of Allergy, Asthma & Immunology*. 128(5):505–11.
14. Tao, R., Li, R., Wang, R. (2021). Skin microbiome alterations in seborrheic dermatitis and dandruff: A systematic review. *Exp Dermatol*. 30(10):1546–53.
15. Baysal, V., Yildirim, M., Ozcanli, C., Ceyhan, A.M. (2004). Itraconazole in the treatment of seborrheic dermatitis: a new treatment modality. *Int J Dermatol*. 43(1):63–6.
16. Elman, S., Hynan, L.S., Gabriel, V., Mayo, M.J. (2010). The 5-D itch scale: a new measure of pruritus. *Br J Dermatol*. 162(3):587–93.
17. Finlay, A.Y., Khan, G.K. (1994). Dermatology Life Quality Index (DLQI)—a simple practical measure for routine clinical use. *Clin Exp Dermatol*. 19(3):210–6.
18. Basra, M.K.A., Fenech, R., Gatt, R.M., Salek, M.S., Finlay, A.Y. (2008). The Dermatology Life Quality Index 1994–2007: a comprehensive review of validation data and clinical results. *Br J Dermatol*. 159(5):997–1035.
19. Yamamoto, T., Takiwaki, H., Arase, S., Ohshima, H. (2008). Derivation and clinical application of special imaging by means of digital cameras and Image J freeware for quantification of erythema and pigmentation. *Skin Res Technol*. 14(1):26–34.
20. Kolecka, A., Khayhan, K., Arabatzis, M., Velegraki, A., Kostrzewa, M., Andersson, A., et al. (2014). Efficient identification of Malassezia yeasts by matrix-assisted laser desorption ionization-time of flight mass spectrometry (MALDI-TOF MS). *Br J Dermatol*. 170(2):332–41.
21. Boiten, W., Absalah, S., Vreeken, R., Bouwstra, J., van Smeden, J. (2016). Quantitative analysis of ceramides using a novel lipidomics approach with three dimensional response modelling. *Biochimica et Biophysica Acta (BBA) - Molecular and Cell Biology of Lipids*. 1861(11):1652–61.
22. Motta, S., Monti, M., Sesana, S., Caputo, R., Carelli, S., Ghidoni, R. (1993). Ceramide composition of the psoriatic scale. *Biochim Biophys Acta*. 1182(2):147–51.

23. Poon, T.S.C., Kuchel, J.M., Badruddin, A., Halliday, G.M., Barnetson, R.StC., Iwaki, H., et al. (2003). Objective Measurement of Minimal Erythema and Melanogenic Doses Using Natural and Solar-simulated Light. *Photochem Photobiol*. 78(4):331–6.
24. Ten Voorde, W., Saghari, M., Boltjes, J., Marieke, |, De Kam, L., Zhuparris, A., et al. (2023). A multimodal, comprehensive characterization of a cutaneous wound model in healthy volunteers. *Exp Dermatol*. 00:1–14.
25. Logger, J.G.M., de Jong, E.M.G.J., Driessen, R.J.B., van Erp, P.E.J. (2020). Evaluation of a simple image-based tool to quantify facial erythema in rosacea during treatment. *Skin Res Technol*. 26(6):804–12.
26. Ohshima, H., Takiwaki, H., Washizaki, K., Ishiko, A., Itoh, M., Kanto, H. (2011). Quantitative evaluation of patch test reactions: a comparison between visual grading and erythema index image analysis. *Skin Res Technol*. 17(2):220–5.
27. Tao, M., Li, M., Zhang, Y., Liu, Y., Jiang, P., Liu, Y., et al. (2023). Objectively quantifying facial erythema in rosacea aided by the ImageJ analysis of VISIA red images. *Skin Res Technol*. 29(1):e13241.
28. Frew, J., Penzi, L., Suarez-Farinas, M., Garcet, S., Brunner, P.M., Czarnowicki, T., et al. (2021). The erythema Q-score, an imaging biomarker for redness in skin inflammation. *Exp Dermatol*. 30(3):377.
29. Oh, Y., Markova, A., Noor, S.J., Rotemberg, V. (2022). Standardized clinical photography considerations in patients across skin tones. *Br J Dermatol*.. 186(2):352–4.
30. Rajabi-Estarabadi, A., Tsang, D.C., Nouri, K., Tosti, A. (2019). Evaluation of positive patch test reactions using optical coherence tomography: A pilot study. *Skin Res Technol*. 25(5):625–30.
31. Odorici, G., Losi, A., Ciardo, S., Pellacani, G., Conti, A. (2018). Non-invasive evaluation of Secukinumab efficacy in severe plaque psoriasis with confocal microscopy and optical coherence tomography: A case report. *Skin Res Technol*. 24(1):160–2.
32. Yélamos, O., Alejo, B., Ertekin, S.S., Villa-Crespo, L., Zamora-Barquero, S., Martinez, N., et al. (2021). Non-invasive clinical and microscopic evaluation of the response to treatment with clobetasol cream vs. calcipotriol/betamethasone dipropionate foam in mild to moderate plaque psoriasis: an investigator-initiated, phase IV, unicentric, open, randomized clinical trial. *J. Eur. Acad. Dermatol. Venereol.*. 35(1):143.
33. Byers, R.A., Maiti, R., Danby, S.G., Pang, E.J., Mitchell, B., Carré, M.J., et al. (2018). Sub-clinical assessment of atopic dermatitis severity using angiographic optical coherence tomography. *Biomed Opt Express*. 9(4):2001.
34. Ha-Wissel, L., Yasak, H., Huber, R., Zillikens, D., Ludwig, R.J., Thaçi, D., et al. (2022). Case report: Optical coherence tomography for monitoring biologic therapy in psoriasis and atopic dermatitis. *Front Med (Lausanne)*. 9:2932.
35. Rissmann, R., Moerland, M., van Doorn, M.B.A. (2020). Blueprint for mechanistic, data-rich early phase clinical pharmacology studies in dermatology. *Br J Clin Pharmacol*. 86(6):1011.
36. Sanders, M.G.H., Nijsten, T., Verlouw, J., Kraaij, R., Pardo, L.M. (2021). Composition of cutaneous bacterial microbiome in seborrheic dermatitis patients: A cross-sectional study. *PLoS One*. 16(5):e0251136.
37. Geoghegan, J.A., Irvine, A.D., Foster, T.J. (2018). Staphylococcus aureus and Atopic Dermatitis: A Complex and Evolving Relationship. *Trends Microbiol*. 26(6):484–97.
38. Tamer, F., Yuksel, M., Sarifakioglu, E., Karabag, Y. (2018). Staphylococcus aureus is the most common bacterial agent of the skin flora of patients with seborrheic dermatitis. *Dermatol Pract Concept*. 8(2):80–4.
39. Findley, K., Oh, J., Yang, J., Conlan, S., Deming, C., Meyer, J.A., et al. (2013). Topographic diversity of fungal and bacterial communities in human skin. *Nature.* 498(7454):367–70.
40. Tao, R., Li, R., Wang, R., Tao, R., Li, R., Wang, R. (2023). Comparative analysis of the facial microbiome between rosacea and seborrheic dermatitis. *Indian J Dermatol Venereol Leprol*. 0(0):1–3.
41. Grice, E.A., Dawson, T.L. (2017). Host–microbe interactions: Malassezia and human skin. *Curr Opin Microbiol*. 40:81–7.
42. Angiolella, L., Rojas, F., Mussin, J., Greco, R., Sosa, M.D.L.A., Zalazar, L., et al. (2020). Biofilm formation, adherence, and hydrophobicity of M. sympodialis, M. globosa, and M. slooffiae from

clinical isolates and normal skin virulence factors of M. sympodialis, M. globosa and M. slooffiae. *Med Mycol*. 58(8):1162–8.
43. Theelen, B., Cafarchia, C., Gaitanis, G., Bassukas, I.D., Boekhout, T., Dawson, T.L. (2018). Malassezia ecology, pathophysiology, and treatment. *Med Mycol*. 56(suppl_1):S10–25.
44. Abdillah, A., Ranque, S. (2021). MalaSelect: A Selective Culture Medium for Malassezia Species. *Journal of Fungi*. 7(10).
45. Prohic, A., Jovovic Sadikovic, T., Krupalija-Fazlic, M., Kuskunovic-Vlahovljak, S. (2016). Malassezia species in healthy skin and in dermatological conditions. *Int J Dermatol*. 55(5):494–504.
46. Angiolella, L., Leone, C., Rojas, F., Mussin, J., Angeles Sosa, M. de los, Giusiano, G. (2018). Biofilm, adherence, and hydrophobicity as virulence factors in Malassezia furfur. *Med Mycol*. 56(1):110–6.
47. Chebil, W., Rhimi, W., Haouas, N., Romano, V., Belgacem, S., Belhadj Ali, H., et al. (2022). Virulence factors of Malassezia strains isolated from pityriasis versicolor patients and healthy individuals. *Med Mycol*. 60(8):60.
48. Tollesson, A., Frithz, A. (1993). Transepidermal water loss and water content in the stratum corneum in infantile seborrhoeic dermatitis. *Acta Derm Venereol*. 73(1):18–20.
49. Suchonwanit, P., Triyangkulsri, K., Ploydaeng, M., Leerunyakul, K. (2019). Assessing Biophysical and Physiological Profiles of Scalp Seborrheic Dermatitis in the Thai Population. *Biomed Res Int*. .
50. Yokose, U., Ishikawa, J., Morokuma, Y., Naoe, A., Inoue, Y., Yasuda, Y., et al. (2020). The ceramide [NP]/[NS] ratio in the stratum corneum is a potential marker for skin properties and epidermal differentiation. *BMC Dermatol*. 20(1).
51. Danso, M., Boiten, W., van Drongelen, V., Gmelig Meijling, K., Gooris, G., el Ghalbzouri, A., et al. (2017). Altered expression of epidermal lipid bio-synthesis enzymes in atopic dermatitis skin is accompanied by changes in stratum corneum lipid composition. *J Dermatol Sci*. 88(1):57–66.
52. Berdyshev, E., Goleva, E., Bissonnette, R., Bronova, I., Bronoff, A.S., Richers, B.N., et al. (2022). Dupilumab significantly improves skin barrier function in patients with moderate-to-severe atopic dermatitis. *Allergy*. 77(11):3388–97.
53. Ito, S., Ishikawa, J., Naoe, A., Yoshida, H., Hachiya, A., Fujimura, T., et al. (2017). Ceramide synthase 4 is highly expressed in involved skin of patients with atopic dermatitis. *J Eur Acad Dermatol Venereol*. 31(1):135–41.
54. Kim, B.K., Shon, J.C., Seo, H.S., Liu, K.H., Lee, J.W., Ahn, S.K., et al. (2022). Decrease of ceramides with long-chain fatty acids in psoriasis: Possible inhibitory effect of interferon gamma on chain elongation. *Exp Dermatol*. 31(2):122–32.
55. Danso, M.O., van Drongelen, V., Mulder, A., van Esch, J., Scott, H., van Smeden, J., et al. (2014). TNF-α and Th2 cytokines induce atopic dermatitis-like features on epidermal differentiation proteins and stratum corneum lipids in human skin equivalents. *J Invest Dermatol*. 134(7):1941–50.
56. Tawada, C., Kanoh, H., Nakamura, M., Mizutani, Y., Fujisawa, T., Banno, Y., et al. (2014). Interferon-γ Decreases Ceramides with Long-Chain Fatty Acids: Possible Involvement in Atopic Dermatitis and Psoriasis. *J Invest Dermatol*.. 134(3):712–8.
57. Berdyshev, E., Goleva, E., Bronova, I., Dyjack, N., Rios, C., Jung, J., et al. (2018). Lipid abnormalities in atopic skin are driven by type 2 cytokines. *JCI Insight*. 3(4).
58. Berdyshev, E., Goleva, E., Bissonnette, R., Bronova, I., Bronoff, A.S., Richers, B.N., et al. (2022). Dupilumab significantly improves skin barrier function in patients with moderate-to-severe atopic dermatitis. *Allergy*. 77(11):3388–97.
59. Uche, L.E., Gooris, G.S., Bouwstra, J.A., Beddoes, C.M. (2019). Barrier Capability of Skin Lipid Models: Effect of Ceramides and Free Fatty Acid Composition. *Langmuir*. 35(47):15376–88.
60. Nădăban, A., Rousel, J., El Yachioui, D., Gooris, G.S., Beddoes, C.M., Dalgliesh, R.M., et al. (2023). The effect of sphingosine and phytosphingosine ceramide ratio on lipid arrangement and barrier functionality in skin lipid models. *J Lipid Res*. 64(8):100400
61. Mojumdar, E.H., Helder, R.W.J., Gooris, G.S., Bouwstra, J.A. (2014). Monounsaturated fatty acids reduce the barrier of stratum corneum lipid membranes by enhancing the formation of a hexagonal lateral packing. *Langmuir*. 30(22):6534–43.
62. Uche, L.E., Gooris, G.S., Bouwstra, J.A., Beddoes, C.M. (2021). Increased Levels of Short-Chain Ceramides Modify the Lipid Organization and Reduce the Lipid Barrier of Skin Model Membranes. *Langmuir*. 37(31):9478–89.

63. Ishikawa, J., Shimotoyodome, Y., Ito, S., Miyauchi, Y., Fujimura, T., Kitahara, T., et al. (2013). Variations in the ceramide profile in different seasons and regions of the body contribute to stratum corneum functions. *Arch Dermatol Res*. 305(2):151–62.
64. Mori, S., Shiraishi, A., Epplen, K., Butcher, D., Murase, D., Yasuda, Y., et al. (2017). Characterization of skin function associated with obesity and specific correlation to local/systemic parameters in American women. *Lipids Health Dis*. 16(1).
65. Rogers, J., Harding, C., Mayo, A., Banks, J., Rawlings, A. (1996). Stratum corneum lipids: the effect of ageing and the seasons. *Arch Dermatol Res*. 288(12):765–70.
66. Pappas, A., Kendall, A.C., Brownbridge, L.C., Batchvarova, N., Nicolaou, A. (2018). Seasonal changes in epidermal ceramides are linked to impaired barrier function in acne patients. *Exp Dermatol*. 27(8):833–6.
67. Voegeli, R., Gierschendorf, J., Summers, B., Rawlings, A. v. (2019). Facial skin mapping: from single point bio-instrumental evaluation to continuous visualization of skin hydration, barrier function, skin surface pH, and sebum in different ethnic skin types. *Int J Cosmet Sci*. 41(5):411–24.
68. Kobayashi, H., Tagami, H. (2004). Distinct locational differences observable in biophysical functions of the facial skin: with special emphasis on the poor functional properties of the stratum corneum of the perioral region. *Int J Cosmet Sci*. 26(2):91–101.
69. Voegeli, R., Rawlings, A. V., Seroul, P., Summers, B. (2015). A novel continuous colour mapping approach for visualization of facial skin hydration and transepidermal water loss for four ethnic groups. *Int J Cosmet Sci*. 37(6):595–605.
70. van Zuuren, E.J., Fedorowicz, Z., Christensen, R., Lavrijsen, A., Arents, B.W.M. (2017). Emollients and moisturisers for eczema. *Cochrane Database Syst Rev*. 2017(2).
71. Mangion, S.E., Mackenzie, L., Roberts, M.S., Holmes, A.M. (2023). Seborrheic dermatitis: topical therapeutics and formulation design. *Eur. J. Pharm. Biopharm.* 185:148–64.
72. Desai, S., McCormick, E., Friedman, A. (2022). An Up-to-Date Approach to the Management of Seborrheic Dermatitis. *J Drugs Dermatol*. 21(12):1373–4.

SUPPLEMENTAL INFORMATION

EXTENDED MATERIAL AND METHODS

Study design and population

This was a cross-sectional study which consisted of one screening and one visit. The study was conducted at the facilities of the Centre for Human Drug Research (Leiden, the Netherlands). Between November 2018 and December 2019, a total of 115 persons were screened for eligibility with the study in- and exclusion criteria. Inclusion criteria included being 18 years or older, SD scored with an Investigators Global Assessment of 2 or 3 with sufficient surface area for all assessments, confirmation of SD by a dermatologist and willingness to refrain from any SD treatments during study participation. Exclusion criteria included the presence of any current or recurrent clinically significant (skin) condition other than SD, recent excessive sun exposure, adapting a different washing routing 1 week prior to screening and the use of SD topical treatments and dandruff shampoo 2 weeks, phototherapy 3 weeks and systemic treatments 4 weeks prior to enrolment. In total, 37 patients were included after successfully passing the screening. All 37 included subjects underwent the visit as planned within 28 days of screening. No formal power calculations were performed to determine group size because of the exploratory nature of the study. Patients were instructed not to wash their face 12 hours preceding the study visit. Non-lesional was defined as an area of skin without any clinical characteristics of SD and was similarly located on the face. Different areas for measurements were chosen on a per-subject basis depending on the availability of sufficient lesional skin and the disqualification of areas due to invasive measurements. These areas have been listed in the supplementary table 2 and 3.

Clinical characteristics

Clinical assessments were performed by trained physicians. The Seborrheic Dermatitis and Severity Index (SDASI) was adapted from Baysal, et al. (2004) (1) to include only the facial extent of SD. Additionally, a 5-point IGA and an estimation of the percentage of affected body surface area (%BSA) were performed. Patient reported outcomes included the average amount of itch experienced by a 0 – 100 Numeric Rating Scale (NRS) itch, the 5-Domain Itch Questionnaire (2) as well as impact of SD on general life by the Dermatology Life Quality Index (DLQI) (3,4). Facial Seborrheic Dermatitis Area and Severity Index (SDASI): Erythema, scaling and papules are scores 0 – 4 with; 0 = none, 1 = mild, 2 = moderate, 3 = severe. The area of involvement is estimated as the fraction of the face with lesional skin and is scored by: 1 = less than 10%, 2 = 11 – 30%, 3 = 31 – 50%, 4 = 51 – 70 and 5 = more than 70%. Erythema, scaling and papule scores are then summed and multiplied by the area score. The scoring is based on the SDASI by Baysal et al. (2004) (1).

Investigator's Global Assessment (IGA): The IGA is a general 5-point scale in which the severity of disease is scored with 0 = clear, 1 = almost clear, 2 = mild, 3 = moderate and 4 = severe. Percentage body surface area affected (%BSA): The area of involvement is estimated using the hand palm method where the surface of a patient's hand equals 1% of the total body surface area.

Standardized photography

Standardized 2D cross-polarized images of the face were taken using a VISIA-CR (Canfield Scientific, New Jersey, United States). Erythema Index calculations were performed based on a method by Yamamoto, et al. (2008) (5). In short, obtained Red Green Blue (RGB) images were split and the R and G channels log transformed using ImageJ (version 1.51h) (6). After subtraction of the R channel with the G channel, brightness was increased by 3 and the mean grey value within a predefined region of interest of 500000 pixels was determined for a lesional and non-lesional area.

Optical Coherence Tomography

Lesional and non-lesional skin was imaged with a Vivosight Dx OCT (Michelson Diagnostics, Kent, United Kingdom). The epidermal thickness, superficial roughness and average epidermal perfusion depth was determined from the resulting scans using the proprietary VivoTools 4.12 software. Individual perfusion-over-depth curves were reviewed and excluded if high superficial levels of perfusion were observed, indicating an invalid measurement in 4 lesional and 4 non-lesional measurements. Epidermal thickness could only be determined in 23 of 37 lesional and 34 of 37 non-lesional measurements because of pronounced epidermal disorganization resulting in troublesome localization of the dermal-epidermal junction.

Microbial analysis by sequencing

Sterile 0.9% NaCl soaked skin swabs (Puritan Sterile Polyester Tipped Applicators, Puritan, Guilford, Maine, United States) were collected by rubbing over a lesional or non-lesional site for 10 seconds while rotating the swab and subsequently stored in DNA/RNA shield lysis buffer and beat beads (Zymo Research, Irvine, California, Unites States) at -80 °C. Swabs were transferred to Baseclear B.V. (Leiden, the Netherlands) for extraction and subsequent sequencing. DNA was extracted using a ZymoBIOMICS DNA Miniprep Kit (Zymo Research) according to manufacturer's instructions. Next-Generation Sequencing for the bacterial and fungal composition was performed using amplification of 16S rRNA region V3-V4 and Internal transcribed spacer region 2 (ITS2), respectively. An Illumina NovaSeq 6000 or MiSeq system was used to generate single- or pair-end sequence reads. FASTQ read sequence files were generated using bcl2fastq2 version 2.18. Primary quality was assessed using the Illumina Chastity filtering and reads containing a PhiX control

signal removed. Quality was finally assessed using the FASTQC quality control tool version 0.11.5. USEARCH version 9.2(7) was used to create pseudoreads and classification of these reads performed based on the alignment with SNAP version 1.0.23 (8) against the RDP database for bacterial (9) and UNITE ITS gene database for fungal classification (10). The resulting list of Operational Taxonomic Units per sample was filtered to genus level and the detected genera included in analysis if it exceeded 1% of the total composition within a sample. Data was presented in the Genome Explorer database (Baseclear B.V., Leiden, the Netherlands) and further processed in Python version 3.8.0 (Python Software Foundation, Wilmington, Delaware, United States) in which microbes contributing <1% of the total were excluded after which their relative abundance at the genus level was determined.

Malassezia culturing

9 cm diameter Agar plates with modified Dixon medium (Mediaproducts B.V., Groningen, the Netherlands) were pressed against a lesional and non-lesional site for 20 seconds. Plates were cultured at 33 °C for up to 21 days at the Microbiology department of the Alrijne Hospital (Leiden, the Netherlands). A sample from each colony forming unit was isolated after positive identification for bacterial or fungal growth through light microscopy. Mycological isolates were transported to the Westerdijk Fungal Biodiversity Institute (Utrecht, the Netherlands) for Malassezia species determination by matrix-assisted laser desorption ionization-time of flight mass spectrometry (MALDI-TOF MS) as described by Kolecka et al. (2014) (11).

Skin barrier integrity by trans-epidermal water loss

Subjects were allowed to acclimatize to controlled environmental conditions (humidity <60%, temperature 22±2 °C) in rested state for at least 15 minutes prior to measurements. An AquaFlux AF200 (Biox Systems Ltd., London, United Kingdom) was used to measure the TEWL of lesional and non-lesional skin. Baseline calibration was performed and TEWL was measured for up to 200 seconds or until a steady state was reached.

Tape stripping procedure

Stratum corneum was harvested by pressing polyphenylene sulfide tape (Nichiban, Tokyo, Japan) to the skin with a D500 D-squame Pressure Instrument (CuDerm Corporation, Dallas, TX, United States) and exerting pressure 5 times. Tapes were transferred to a cutting board with the glue side up. 16 mm diameter holes were punched within the region that was pressed against the skin. The individual punched out tape samples were stored in 20 ml vials with 1.5 ml of chloroform:methanol (2:1) at -20 °C before extraction.

Ceramide analysis by liquid chromatography-mass spectrometry

HPLC grade chloroform (Honeywell, Charlotte, North Carolina, United States), UPLC grade Methanol (Biosolve, Valkenswaard, the Netherlands), UPLC grade heptane (LiChorSolv, Merck, Darmstadt, Germany), UPLC grade isopropyl alcohol (Biosolve, Valkenswaard, the Netherlands), UPLC grade ethanol (Biosolve, Valkenswaard, the Netherlands), reagent grade potassium chloride (Sigma Aldrich, Saint-Louis, Missouri, USA) and ultrapure water from a Milli-Q Advantage A10 system (Merck, Darmstadt, Germany) were used. Synthetic ceramides and deuterated standards were purchased from Avanti Polar Lipids (Alabaster, Alabama, United States) or kindly provided by Evonik (Essen, Germany).

Extraction of tape strips and analysis of the ceramide profile was performed as described Boiten et al. (2016) (12). In short, individual tape samples were stored in 1.5 ml of chloroform:methanol (2:1) in a 20 ml glass vial and stored at -20 °C before analysis. Tapes were extracted by shaking the tape samples in an IKA S4000 rotary shaker at 120 rounds per minute at 40 °C for one hour. Solvent was isolated and shaking repeated three times with 1 ml of different solvent mixtures; chloroform:methanol:water (1:2:0.5), chloroform:methanol (1:1) and heptane:isopropylalcohol (1:1). Solvent was isolated each time and pooled with the previous collected organic solvent. 4 ml of 0.25M KCl was added to the pooled solvent and phase separation achieved overnight. The organic layer was isolated and washed with the addition of 4 ml chloroform. The isolated organic layer was combined with the washing solvent and filtered through 0.45 µm PVDF syringe filters (Grace, Deerfield IL, USA). Samples were transferred to 1.5 ml HPLC vials and reconstituted in 750 µl chloroform:methanol (2:1). 225 µl of this stock was transferred to a separate HPLC vial, dried, and reconstituted in 60 µl heptane:chloroform:methanol (95:2.5:2.5) containing 10 µM CER[N(24deu)S(18)] for analysis by UPLC-MS. Separation was achieved by a 5 µl injection using an Acquity UPLC H-class (Waters, Milford, MA, USA) and a normal phase PVA-silica column (5 µm particles, 100 × 2.1 mm i.d.) (YMC, Kyoto, Japan) over a gradient from 98% heptane and 2% heptene:isopropylalcohol:ethanol (2:1:1) to 50% heptane and 50% heptene:isopropylalcohol:ethanol (2:1:1) at a flow rate of 0.8 ml/min. Detection was performed using atmospheric pressure chemical ionization (APCI) on a XEVO TQ-S mass spectrometer (Waters, Milford, MA, USA) in positive ion mode scanning from 350 to 1200 m/z. Quality control samples from combined stratum corneum extracts and standard calibration curves containing 50, 20, 10, 5, 2, 1, 0.5, 0 µM of several ceramides (Cer[NS, NdS, NP, AS, EOS and EOP] in triplicate were added to the run. Responses of 2 out of 64 samples were below the limit of detection and therefore excluded from analysis.

Peaks at the ceramides monoisotopic mass were integrated using TargetLynx V4.1 (Waters, Milford, MA, USA) and Area Under the Curve (AUC) responses corrected for the internal standard in Excel (Microsoft 365, Redmond, Washington, United States). The monoisotopic AUC was further corrected by the degree of water loss as determined from quality control samples. AUC were further corrected by the ceramides theoretic 13C

isotope distribution. Using the calibration curves, correction for increased responses at higher masses was performed. This corrected response per ceramide was converted to relative data using the total corrected AUC and calculations were made after grouping individual ceramides by class or chain lengths for further graphing.

Sebum measurements

Lesional and non-lesional skin was measured using a Sebumeter SM815 (Courage+Khazaka, Köln, Germany). The Sebumeter was calibrated before a patient was measured. Three measurements were performed next to each other on the same predefined lesional or non-lesional site. The average of this triplicate measurement was used for graphing.

Statistical analysis

Data visualization and statistical testing was performed using Prism 9 (Graphpad Software, San Diego, California, United States). 2-way ANOVA, or a mixed effects model in the case of missing data points, was performed using Bonferroni's multiple comparison test in the case of multiple variables and paired t-test in the case of two variables. P-values are denoted as *: P≤0.05, **: P≤0.01, ***: P≤0.001. Integrative data graphing by principal component analysis (PCA) and radar plot has been performed through Python version 3.8.0 (Python Software Foundation, Wilmington, Delaware, United States). PCA analysis of the ceramides composition was performed using relative individual ceramide abundance as percentage of all detected saturated ceramides, with values below the limit of quantification set to 0 in order to prevent missing datapoints and allow for PCA analysis. Multimodal integration through PCA was performed on all the data presented in the figures of this paper with mean imputation in the case of missing data, but without epidermal thickness data due to a high amount of data not missing at random in this set as higher epidermal disorganization was more evident in lesional skin. Radar charts using min-max scaling were used to visualize differences between lesional and non-lesional skin in an integrative and descriptive manner. Data used in generation of the ceramide PCA, integrative PCA and integrative radar plot is added as supplemental information.

SUPPLEMENTAL FIGURES

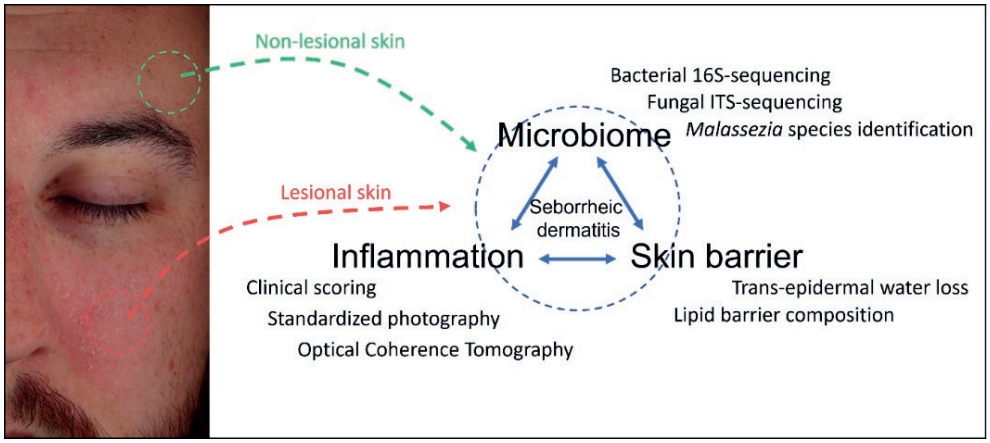

Figure S1. Clinical presentation of a seborrheic dermatitis patient and overview of the study setup showing the assessments performed on lesional and non-lesional skin and the interdependency of inflammation, microbiome and barrier function. Note that the locations indicated are examples of lesional and non-lesional skin and can differ between subjects based on the availability of affected skin as listed in the supplemental data.

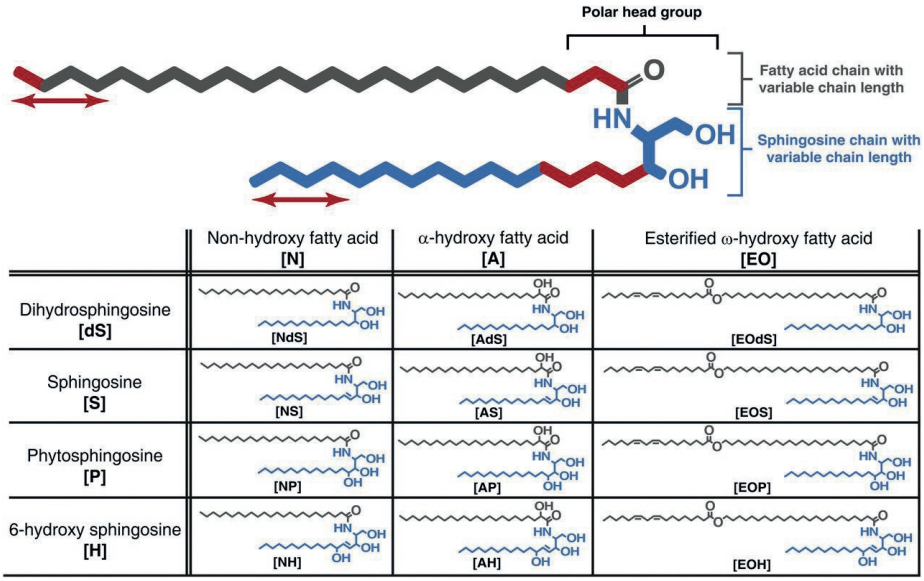

Figure S2. General structure of a ceramide composed of a sphingoid base coupled to a fatty acid chain. The carbon chains attached to the polar head group can vary in length. Differences in the ceramide headgroup architecture is indicated using the naming convention conceived by Motta *et al.* (1993). This image was adapted from Janssens *et al.* (2012) (13).

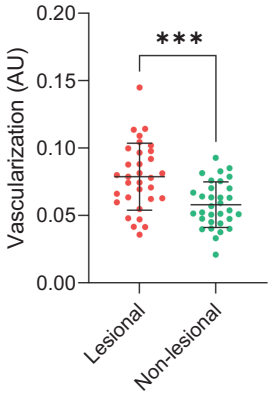

Figure S3. Average vascularization between 0.15 mm up to and including 0.25 mm of lesional and non-lesional skin as determined by optical coherence tomography.

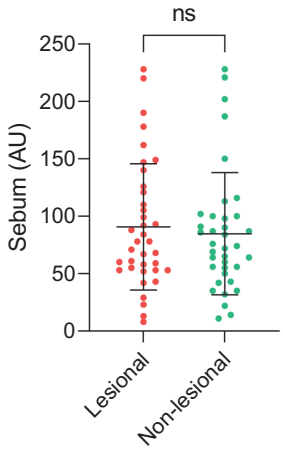

Figure S4. Sebum levels on lesional and non-lesional skin. Datapoints represent the average value of a triplicate measurement.

Table S1. Overview of the location that assessments were performed. Imaging includes both the Erythema Index as determined through standardized 2D-photograpy with VISIA and Optical Coherence Tomography. Lesional and non-lesional sites are indicated with the suffix "*_L*" and "*_NL*", respectively. The table is continued in supplemental table 2.

Subject	Lesional Erythema and OCT	Non-lesional Erythema and OCT	Lesional TEWL	Non-lesional TEWL
1	Nosebridge	Left forehead	Nosebridge	Right forehead
2	Right nosefold	Right forehead	Right nosefold	Right forehead
3	Right nosefold	Right cheek	Right nosefold	Right cheek
4	Left nosefold	Right forehead	Left nosefold	Right forehead
5	Right nosefold	Right cheek	Left nosefold	Right cheek
6	Right nosefold	Left forehead	Right nosefold	Left forehead
7	Left forehead	Right cheek	Left forehead	Right cheek
8	Right nosefold	Right forehead	Right nosefold	Right forehead
9	Right nosefold	Right forehead	Right nosefold	Right forehead
10	Right nosefold	Right lower eyelid	Right nosefold	Right lower eyelid
11	Chin	Right forehead	Right nosefold	Right forehead
12	Right nosefold	Right forehead	Right nosefold	Right forehead
13	Right nosefold	Right forehead	Right nosefold	Right forehead
14	Right upper lip	Right forehead	Right upper lip	Right forehead
15	Right eyebrow, upper	Right cheek	Right eyebrow, upper	Right cheek
16	Nosebridge	Right cheek	Nosebridge	Right cheek
17	Right nosefold	Left forehead	Right nosefold	Left forehead
18	Left nosefold	Right forehead	Left nosefold	Right forehead
19	Right nosefold	Right forehead	Right nosefold	Right forehead
20	Right nosefold	Right cheek	Right nosefold	Right cheek
21	Left upper lip	Left forehead	Left upper lip	Left forehead
22	Right nosefold	Right forehead	Right nosefold	Right forehead
23	Right nosefold	Left forehead	Right nosefold	Left forehead
24	Right nosefold	Right forehead	Right nosefold	Right forehead
25	Right nosefold	Right forehead	Right nosefold	Right forehead
26	Right nosefold	Left forehead	Right nosefold	Left forehead
27	Right forehead	Left Cheek	Right forehead	Left Cheek
28	Left nosefold	Right cheek	Left nosefold	Right cheek
29	Right nosefold	Right forehead	Right nosefold	Right forehead
30	Nosebridge	Right cheek	Nosebridge	Right cheek
31	Left forehead	Left Cheek	Left forehead	Left Cheek

32	Left nosefold	Left Cheek	Left nosefold	Left Cheek
33	Right nosefold	Right cheek	Right nosefold	Right cheek
34	Left nosefold	Left Cheek	Left nosefold	Left Cheek
35	Left nosefold	Left forehead	Left nosefold	Left forehead
36	Left nosefold	Right forehead	Left nosefold	Right forehead
37	Right nosefold	Right forehead	Right nosefold	Right forehead

Table S2. Overview of the location that assessments were performed. Imaging includes both the Erythema Index as determined through standardized 2D-photograpy with VISIA and Optical Coherence Tomography. Lesional and non-lesional sites are indicated with the suffix "*_L*" and "*_NL*", respectively. This is a continuation of supplemental table 1.

Subject	Lesional Swab location	Non-lesional Swab location	Lesional agar plates	Non-lesional agar plates
1	Nosebridge	Right forehead	Nosebridge	Left Cheek
2	Right nosefold	Right cheek	Nosebridge	Right forehead
3	Right nosefold	Right cheek	Left nosefold	Left Cheek
4	Left nosefold	Nosebridge	Left nosefold	Right forehead
5	Right nosefold	Left lower lip	Central forehead	Left lower eyelid
6	Right cheekbone	Left Cheekbone	Left nosefold	Right forehead
7	Right nosefold	Right cheek	Left forehead	Right cheek
8	Right nosefold	Right cheek	Nosebridge	Right forehead
9	Left nosefold	Left forehead	Left nosefold	Right forehead
10	Right upper lip	Right cheek	Left nosefold	Left Cheek
11	Left nosefold	Right forehead	Left Cheek	Left forehead
12	Right lower lip	Right forehead	Left lower lip	Left forehead
13	Right nosefold	Right forehead	Left nosefold	Left forehead
14	Left upper lip	Left forehead	Left eyebrow, upper	Right forehead
15	Left nosefold	Right cheek	Nosebridge	Left Cheek
16	Left Cheek	Right cheek	Nosebridge	Chin
17	Nosebridge	Left Cheek	Left nosefold	Right forehead
18	Right nosefold	Left Cheekbone	Left nosefold	Right forehead
19	Left nosefold	Right forehead	Right cheek	Left forehead
20	Left nosefold	Left forehead	Nosebridge	Left Cheek
21	Nosebridge	Left Cheek	Right upper lip	Right forehead
22	Left nosefold	Left forehead	Right lower lip	Left Cheek
23	Nosebridge	Left Cheek	Left nosefold	Right forehead
24	Left nosefold	Left forehead	Right cheek	Left Cheek

25	Left nosefold	Left forehead	Left nosefold	Left Cheek
26	Right nosefold	Left forehead	Nosebridge	Right cheekbone
27	Left Cheekbone	Left Cheek	Nosebridge	Left Cheek
28	Left nosefold	Right cheek	Nosebridge	Right cheekbone
29	Right nosefold	Left forehead	Right lower lip	Left forehead
30	Left nosefold	Left Cheek	Nosebridge	Left Cheek
31	Right forehead	Left Cheek	Left forehead	Right cheek
32	Nosebridge	Right cheek	Left nosefold	Left Cheek
33	Left nosefold	Left Cheek	Nosebridge	Right cheek
34	Nosebridge	Right cheekbone	Right nosefold	Left Cheek
35	Nosebridge	Right forehead	Right nosefold	Right cheek
36	Left upper lip	Right forehead	Left nosefold	Left Cheek
37	Chin	Right forehead	Left nosefold	Right forehead

Table S3. Overview of the location that assessments were performed. Imaging includes both the Erythema Index as determined through standardized 2D-photograpy with VISIA and Optical Coherence Tomography. Lesional and non-lesional sites are indicated with the suffix "*_L*" and "*_NL*", respectively. This is a continuation of supplemental table 1 and 2.

Subject	Lesional tape stripping	Non-lesional tape stripping	Lesional sebum measurement	Non-lesional sebum measurement
1	Right nosefold	Right cheek	Nosebridge	Right forehead
2	Right nosefold	Left forehead	Left nosefold	Right forehead
3	Right nosefold	Left forehead	Right nosefold	Right cheekbone
4	Right nosefold	Left forehead	Left nosefold	Right forehead
5	Left nosefold	Right cheek	Left nosefold	Right cheekbone
6	Right nosefold	Left forehead	Right nosefold	Left forehead
7	Left forehead	Right forehead	Left forehead	Right cheekbone
8	Right nosefold	Left forehead	Right nosefold	Right forehead
9	Right nosefold	Right cheek	Right nosefold	Right forehead
10	Left upper lip	Left forehead	Right nosefold	Left forehead
11	Right nosefold	Right cheek	Right nosefold	Right forehead
12	Left eyebrow, upper	Right cheekbone	Right nosefold	Right forehead
13	Nosebridge	Left forehead	Right nosefold	Right forehead
14	Right upper lip	Right cheekbone	Right lip, upper	Right eyebrow, upper
15	Left eyebrow, upper	Left Cheek	Right eyebrow, upper	Right cheekbone
16	Right forehead	Left Cheek	Nosebridge	Right cheekbone

17	Right nosefold	Left forehead	Right nosefold	Left forehead
18	Nosebridge	Left forehead	Left forehead	Right forehead
19	Left nosefold	Left Cheekbone	Right cheekbone	Right forehead
20	Right nosefold	Right cheek	Right nosefold	Right cheek
21	Left upper lip	Left forehead	Left forehead	Left forehead
22	Left lower lip	Right cheekbone	Right nosefold	Right forehead
23	Left nosefold	Right forehead	Right nosefold	Left forehead
24	Left nosefold	Left forehead	Right nosefold	Left nosefold
25	Nosebridge	Left forehead	Right nosefold	Right forehead
26	Right nosefold	Right forehead	Right nosefold	Left forehead
27	Right cheekbone	Right cheek	Left cheek	Right forehead
28	Right nosefold	Right cheek	Left forehead	Right cheekbone
29	Left lower lip	Left Cheek	Right nosefold	Right forehead
30	Right nosefold	Right cheek	Nosebridge	Right cheek
31	Right forehead	Left Cheek	Left forehead	Left cheekbone
32	Right nosefold	Right forehead	Left nosefold	Left cheek
33	Right nosefold	Right cheekbone	Right nosefold	Left cheek
34	Left nosefold	Right cheek	Left forehead	Left cheek
35	Left nosefold	Left forehead	Left forehead	Left forehead
36	Right nosefold	Right cheek	Left nosefold	Right forehead
37	Right nosefold	Right cheekbone	Right nosefold	Right forehead

PCA loadings

Table S4. The loadings per parameter used in the generation of the Principal Component Analysis in figure 4A.

	Principal component 1 (36.78%)			Principal component 2 (11.51%)	
	Parameter	**Loading**		**Parameter**	**Loading**
1	Cer[NS]	0.304353	**1**	Cer[OS]	0.377582
2	Ratio Cer[NS:NP]	0.291921	**2**	Cer[OP]	0.337539
3	Cer[AS]	0.291615	**3**	Cer[OH]	0.329363
4	Cer[NSc34]	0.251295	**4**	Cer[EOdS]	0.242378
5	*Staphylococcus* (%)	0.207942	**5**	Fungal Diversity	0.214079
6	Trans-epidermal water loss	0.186069	**6**	Bloodflow at 0.2 mm	0.170678
7	Roughness	0.183875	**7**	Erythema	0.170665
8	MUCer[NS]	0.182895	**8**	Ratio Cer[NS:NP]	0.168114
9	Erythema	0.143098	**9**	Bloodflow at 0.25 mm	0.16635
10	*Malassezia* (%)	0.028224	**10**	Cer[EOH]	0.162232
11	Bloodflow at 0.15 mm	0.004897	**11**	Cer[EOS]	0.161557
12	Bloodflow at 0.35 mm	0.003023	**12**	Bloodflow at 0.15 mm	0.158108
13	Bloodflow at 0.3 mm	-0.00488	**13**	Bloodflow at 0.3 mm	0.156788
14	Bloodflow at 0.2 mm	-0.0056	**14**	Bloodflow at 0.35 mm	0.145911
15	Cer[AdS]	-0.00785	**15**	Bloodflow at 0.1 mm	0.130806
16	Bloodflow at 0.25 mm	-0.01004	**16**	Cer[AH]	0.128493
17	Bloodflow at 0.1 mm	-0.01428	**17**	Trans-epidermal water loss	0.116807
18	Cer[AH]	-0.02809	**18**	Cer[AS]	0.116675
19	Bacterial Diversity	-0.02977	**19**	MUCer[NS]	0.109013
20	Fungal Diversity	-0.06081	**20**	Cer[NS]	0.088148
21	Cer[NdS]	-0.07766	**21**	Cer[EOP]	0.039438
22	Cer[NH]	-0.08445	**22**	Cer[NH]	0.019096
23	Cer[OS]	-0.11084	**23**	Roughness	-0.00196
24	Cer[EOdS]	-0.11781	**24**	Cer[AdS]	-0.02022
25	Cer[AP]	-0.12997	**25**	Cer[NSc34]	-0.05328
26	Cer[OP]	-0.14308	**26**	*Staphylococcus* (%)	-0.07786
27	Cer[OH]	-0.18532	**27**	Bacterial Diversity	-0.09176
28	Cer[EOS]	-0.22501	**28**	Carbon chain length	-0.13019
29	Cer[NP]	-0.22817	**29**	Cer[AP]	-0.15411
30	Cer[EOH]	-0.24775	**30**	*Malassezia* (%)	-0.18649
31	Cer[EOP]	-0.26718	**31**	Cer[NdS]	-0.24213
32	Carbon chain length	-0.39401	**32**	Cer[NP]	-0.24222

SUPPLEMENTARY REFERENCES

1. Baysal, V., Yildirim, M., Ozcanli, C., Ceyhan, A.M. (2004). Itraconazole in the treatment of seborrheic dermatitis: a new treatment modality. *Int J Dermatol*. 43(1):63–6.
2. Elman, S., Hynan, L.S., Gabriel, V., Mayo, M.J. (2010). The 5-D itch scale: a new measure of pruritus. *Br J Dermatol*. 162(3):587–93.
3. Finlay, A.Y., Khan, G.K. (1994). Dermatology Life Quality Index (DLQI)—a simple practical measure for routine clinical use. *Clin Exp Dermatol*. 19(3):210–6.
4. Basra, M.K.A., Fenech, R., Gatt, R.M., Salek, M.S., Finlay, A.Y. (2008). The Dermatology Life Quality Index 1994–2007: a comprehensive review of validation data and clinical results. *British Journal of Dermatology*. 159(5):997–1035.
5. Yamamoto, T., Takiwaki, H., Arase, S., Ohshima, H. (2008). Derivation and clinical application of special imaging by means of digital cameras and Image J freeware for quantification of erythema and pigmentation. *Skin Res Technol*. 14(1):26–34.
6. Rasband, W.S. ImageJ. Bethesda, Maryland, USA: U.S. National Institutes of Health;
7. Edgar, R.C. (2010). Search and clustering orders of magnitude faster than BLAST. *Bioinformatics*. 26(19):2460–1.
8. Zaharia, M., Bolosky, W.J., Curtis, K., Fox, A., Patterson, D., Shenker, S., et al. (2011). Faster and More Accurate Sequence Alignment with SNAP.
9. Cole, J.R., Wang, Q., Fish, J.A., Chai, B., McGarrell, D.M., Sun, Y., et al. (2014). Ribosomal Database Project: data and tools for high throughput rRNA analysis. *Nucleic Acids Res*. 42(Database issue).
10. Abarenkov, K., Nilsson, R.H., Larsson, K.H., Alexander, I.J., Eberhardt, U., Erland, S., et al. (2010). The UNITE database for molecular identification of fungi – recent updates and future perspectives. *New Phytologist*. 186(2):281–5.
11. Kolecka, A., Khayhan, K., Arabatzis, M., Velegraki, A., Kostrzewa, M., Andersson, A., et al. (2014). Efficient identification of Malassezia yeasts by matrix-assisted laser desorption ionization-time of flight mass spectrometry (MALDI-TOF MS). *British Journal of Dermatology*. 170(2):332–41.
12. Boiten, W., Absalah, S., Vreeken, R., Bouwstra, J., van Smeden, J. (2016). Quantitative analysis of ceramides using a novel lipidomics approach with three dimensional response modelling. *Biochimica et Biophysica Acta (BBA) - Molecular and Cell Biology of Lipids*. 1861(11):1652–61.
13. Janssens, M., van Smeden, J., Gooris, G.S., Bras, W., Portale, G., Caspers, P.J., et al. (2012). Increase in short-chain ceramides correlates with an altered lipid organization and decreased barrier function in atopic eczema patients. *J Lipid Res*. 53(12):2755–66.